Dinitrogen Reduction to Ammonium at Rhenium Utilizing Light and Proton-Coupled Electron Transfer

Quinton J. Bruch,[†] Gannon P. Connor,[‡] Chun-Hsing Chen,[†] Patrick L. Holland,[‡] James M. Mayer,[‡] Faraj Hasanayn,[§*] Alexander J. M. Miller[†*]

[†] *Department of Chemistry, University of North Carolina at Chapel Hill, Chapel Hill, North Carolina 27599–3290, United States*

[‡] *Department of Chemistry, Yale University, New Haven, Connecticut 06520, United States*

[§] *Department of Chemistry, American University of Beirut, Beirut 1107 2020, Lebanon*

ABSTRACT: The direct scission of the triple bond of dinitrogen (N_2) by a metal complex is an alluring entry point into the transformation of N_2 to ammonia (NH_3) in molecular catalysis. Reported herein is a pincer-ligated rhenium system that reduces N_2 to NH_3 via a well-defined reaction sequence involving reductive formation of a bridging N_2 complex, photolytic N_2 splitting, and proton-coupled electron transfer (PCET) reduction of the metal-nitride bond. The new complex (PONOP)$ReCl_3$ (PONOP = 2,6-bis(diisopropylphosphinito)pyridine) is reduced under N_2 to afford the *trans,trans*-isomer of the bimetallic complex [(PONOP)$ReCl_2$]$_2$(μ-N_2) as an isolable kinetic product that isomerizes sequentially upon heating into the *trans,cis* and *cis,cis* isomers. All isomers are inert to thermal N_2 scission, and the *trans,trans*-isomer is also inert to photolytic N_2 cleavage. In striking contrast, illumination of the *trans,cis* and *cis,cis*-isomers with blue light (405 nm) affords the octahedral nitride complex *cis*-(PONOP)Re(N)Cl_2 in 47% spectroscopic yield and 11% quantum yield. The photon energy drives an N_2 splitting reaction that is thermodynamically unfavorable under standard conditions, producing a nitrido complex that reacts with SmI_2/H_2O to produce a rhenium tetrahydride complex (38% yield) and furnish ammonia in 74% yield.

1. INTRODUCTION

The 1908 discovery of a catalytic process for the hydrogenation of dinitrogen (N_2) to ammonia (NH_3) revolutionized global agriculture.[1] The H_2 required for the Haber-Bosch process is generated by co-located hydrocarbon steam reforming plants that release massive amounts of CO_2, leading to serious concerns about the long-term environmental impact of NH_3 synthesis.[1] A sustainable alternative to the Haber-Bosch process could involve photo- and/or electrochemical reduction of N_2 under mild conditions using water as a source of protons and electrons.[2–4] Tailored molecular catalysts have shown promise in driving NH_3 synthesis under ambient conditions utilizing chemical reductants and acids, often enabled by insight into the mechanism of N_2 activation and reduction.[5–8]

Three types of mechanistic pathways for the $6H^+/6e^-$ reduction of N_2 to NH_3 are shown in Scheme 1.[5,7,8] In the "distal" pathway (or Chatt cycle), the nitrogen atom furthest from the metal is fully reduced to NH_3 before the metal-bound nitrogen atom receives any hydrogen atoms (Scheme 1, blue).[5,7,9,10] In the "alternating" pathway, hydrogen equivalents are added sequentially to the distal and the proximal nitrogen atoms, leading to metal-bound diazene and hydrazine intermediates (Scheme 1, purple).[5,7] Most molecular catalysts for N_2 reduction are proposed to proceed via one of these two pathways.[5,7]

An alternative pathway involves direct cleavage of the N≡N triple bond to furnish metal nitride complexes followed by proton/electron transfers to form NH_3 (Scheme 1, red).[8] The N_2 cleavage pathway to NH_3 has only rarely been observed in molecular systems. Holland showed that bridging Fe nitrides derived from N_2 splitting[11] can be converted to NH_3 through a series of protonation and reduction steps.[12] An N_2 splitting mechanism has also been proposed by Nishibayashi in the catalytic reduction of N_2 to NH_3 using (pincer)Mo complexes.[13–15] While the N_2 splitting pathway has been a fascinating target since the first report of molecular N_2 splitting in 1995,[16] well-defined molecular systems capable of converting N_2 to NH_3 via direct splitting of the N≡N bond have encountered two main challenges.

Scheme 1. Three general mechanistic pathways for N_2 reduction to NH_3.

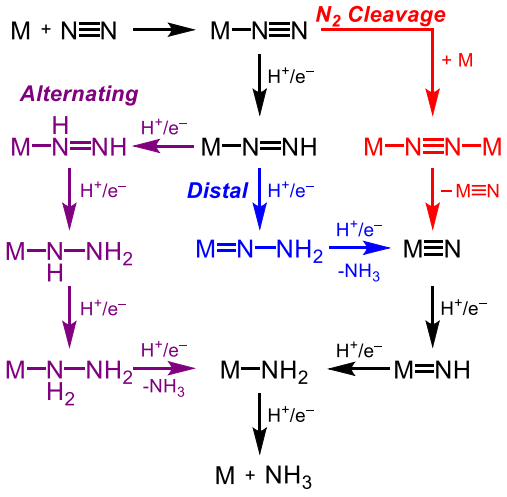

First, molecular systems capable of splitting the strong bond of N_2 into nitrides remain rare. One way to render N≡N bond splitting thermodynamically favorable is to form nitrides that bridge multiple metal centers.[12,17–22] Alternatively, transition metal

complexes with the appropriate electronic structure to support strong metal–nitride multiple bonds can form terminal nitrides from N_2. Following the lead discovery of Cummins (**A**, Figure 1), several molybdenum complexes have proven capable of thermal and photochemical N_2 cleavage.[13–16,23–28] More recently, Schneider reported the first examples of thermal and photochemical N_2 splitting reactions at rhenium to form nitride complexes **B** and **C** (Figure 1), respectively.[29,30]

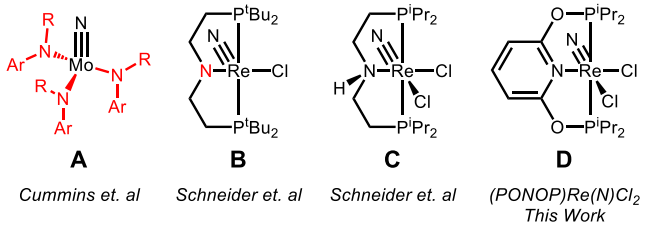

Figure 1. Selected N_2-derived terminal nitrides **A**,[16] **B**,[29] **C**,[30] and **D**. Sites of ligand protonation highlighted in red.

A second challenge is that N_2-derived nitride complexes generally have been resistant to N–H bond formation, with unproductive protonation often occurring at supporting ligands.[23,29] For rhenium complex **B** (Figure 1), for example, protonation occurs at the central amide donor, resulting in a cationic rhenium nitride product.[29] Although elegant syntheses of nitriles from N_2-derived rhenium nitride complexes has been achieved,[30,31] the complete transformation from N_2 to NH_3 at rhenium has not been reported to date.

We sought to overcome the challenges associated with the reduction of N_2-derived nitrides by supporting rhenium complexes with the pincer ligand bis(diisopropylphosphinito)pyridine (PONOP).[32,33] The PONOP ligand offers no obvious alternative sites of protonation, which could focus the reactivity on the rhenium nitride fragment. The neutral pincer ligand featuring oxygen substituents was also expected to render rhenium complexes accessible to reduction at milder potentials.

Herein we report a reaction sequence that converts N_2 to NH_3 using PONOP-supported rhenium complexes. The new octahedral complex (PONOP)$ReCl_3$ undergoes reductive N_2 binding assisted by halide abstraction. The resulting binuclear bridging N_2 complex must isomerize to a configuration that supports photolytic cleavage to a terminal rhenium nitride. Formation of NH_4^+ is observed upon treatment of the nitride complex with SmI_2/H_2O, resulting in the first example of rhenium-mediated fixation of N_2 in the form of NH_3. The ability to isolate intermediates enabled direct experimental and computational studies of individual steps, which provides insight into the factors that control N_2 cleavage reactivity and PCET nitride reduction. With the N_2 cleavage pathway recently proposed in catalytic NH_3 synthesis by Mo pincer complexes,[13,15,24,34] such mechanistic insight may prove broadly relevant to catalyst development.

2. RESULTS AND DISCUSSION

2.1 Reduction and N_2 Binding Steps. In order to explore reductive N_2 binding, new Re^{III} complexes of PONOP were synthesized. Heating a tetrahydrofuran (THF) suspension of $ReCl_3(PPh_3)_2(MeCN)$ with PONOP at 70 °C for 16 h afforded the octahedral complex (PONOP)$Re^{III}Cl_3$ (**1**) in 90% yield. The structure of **1** was determined by single-crystal X-ray diffraction (XRD) (Figure 2, blue). The room temperature magnetic moment of **1** in THF-d_8, μ_{eff} = 1.40 μ_B, is significantly lower than the expected spin-only value for an S = 1 system (2.83 BM), which is consistent with temperature-independent paramagnetism (TIP) exhibited by rhenium(III) compounds.[35,36] The NMR spectral features of **1** also indicate TIP, with sharp peaks spanning a range of 30 ppm across the ^{1}H NMR spectrum, and a sharp singlet at –1571 ppm in the $^{31}P\{^1H\}$ spectrum.[30,36] Cyclic voltammetry (CV) of **1** in THF revealed a reversible one-electron reduction, $E_{1/2}$ = –1.23 V vs $Fc^{+/0}$. This reduction is anodically shifted by more than 600 mV relative to the reduction potential of (HPNP^{iPr})$ReCl_3$ (**C** in Figure 1, HPNP^{iPr} = HN($CH_2CH_2P(^iPr)_2)_2$).[30] The relative ease of reduction of **1** is attributed to the PONOP ligand being substantially less electron-donating than HPNP^{iPr}.

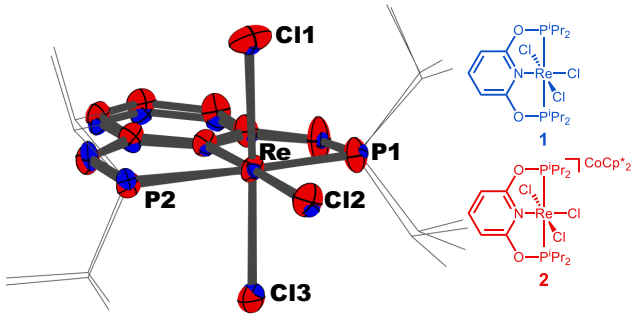

Figure 2. Overlay of structural representations of (PONOP)$Re^{III}Cl_3$ (**1**, blue) and [$CoCp^*_2$][(PONOP)$Re^{II}Cl_3$] (**2**, red) derived from X-ray diffraction analysis. Hydrogen atoms and counter ions omitted for clarity. See SI Section VIII for bond lengths and angles.

The reversible electrochemical response of **1** is consistent with formation of a stable trichlororhenate(II) salt. Indeed, treating an orange THF solution of **1** with $CoCp^*_2$ ($E_{1/2}$ = –1.96 V vs. $Fc^{+/0}$)[37] resulted in immediate and near quantitative conversion to [$CoCp^*_2$][(PONOP)$Re^{II}Cl_3$] (**2**), as confirmed by XRD analysis (Figure 2, Scheme 2; Cp* is pentamethylcyclopentadienyl). Reduction of **1** also proceeds rapidly with the milder and less lipophilic reductant $CoCp_2$ ($E_{1/2} \approx$ –1.3 V vs. $Fc^{+/0}$), but yields a product that is insoluble in most organic solvents.[38] The reduction of **1** to form stable trichloride complex salt **2** contrasts the reactivity of (HPNP^{iPr})$ReCl_3$, which loses chloride rapidly upon reduction.[30]

The isolable monomeric reduced complex **2** presented an opportunity to study the electronic structure of an intermediate that was expected to be a direct precursor to N_2 binding and

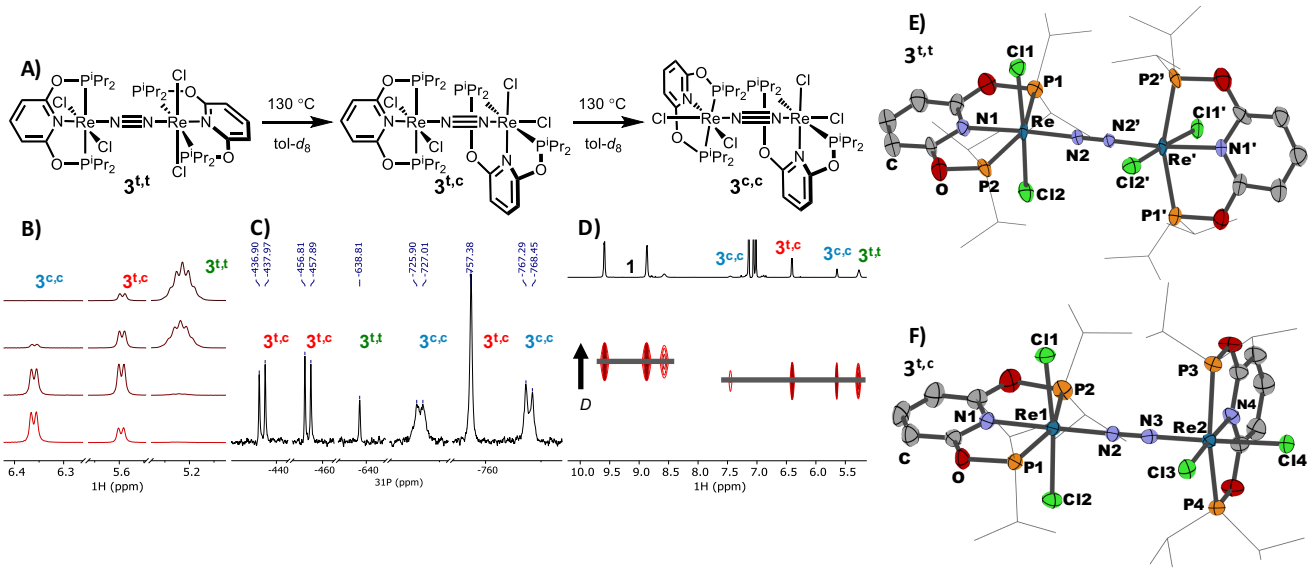

Figure 3. (A) Thermal isomerization of $\mathbf{3^{t,t}}$. (B) ^{1}H NMR spectra during isomerization of $\mathbf{3^{t,t}}$ to $\mathbf{3^{t,c}}$ and $\mathbf{3^{c,c}}$ at 0 h, 0.5 h, 1 h, and 6 h monitoring isopropyl methyl ($\mathbf{3^{t,c}}$ and $\mathbf{3^{c,c}}$) and isopropyl methine ($\mathbf{3^{t,t}}$) resonances. (C) ^{31}P{^{1}H} NMR spectrum at 1 h. (D) DOSY analysis of a 1:1:1:1 mixture of $\mathbf{1}$:$\mathbf{3^{t,t}}$:$\mathbf{3^{t,c}}$:$\mathbf{3^{c,c}}$, y-axis plots the diffusion coefficient *D*. (E) Structural representation of $\mathbf{3^{t,t}}$ from XRD. (F) Structural representation of $\mathbf{3^{t,c}}$ determined by XRD. See SI Section VIII for details.

activation. The rhenium trichloride anion in **2** adopts a pseudo-octahedral structure, with slightly elongated Re–Cl bonds and slightly compressed Re–P bonds relative to **1** (Figure 2). The spectroscopic features of **2** are consistent with a d^5 paramagnetic Re^{II} species. The ^{1}H NMR spectrum features extremely broad, paramagnetically shifted resonances, and a broad, isotropic signal (g = 2.27) is observed in the solid-state EPR spectrum measured at 298 K (Figure S35).[39,40] The computed singly occupied molecular orbital (SOMO) in **2** is dominated by the metal d_{xz} atomic orbital (AO) aligned along the plane of the pincer ligand with minor out-of-phase π-mixing with the chloride ligands (See SI Section XVI for computational details). Accordingly, the computed spin density on the metal is 0.8 e^-, further consistent with a low-spin Re^{II} formulation. Solutions of **2** in THF-d_8 decompose to a mixture of unidentifiable and NMR silent products over the course of several days at room temperature (or several hours at 70 °C).

Scheme 2. Synthesis of **2** and $\mathbf{3^{t,t}}$.

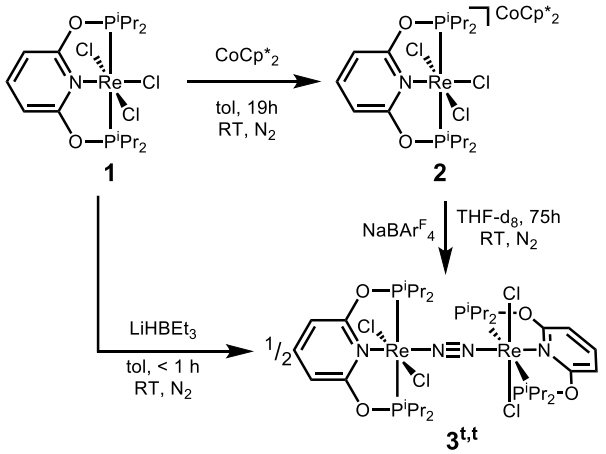

To open a coordination site at Re for reaction with N_2, solutions of **2** in THF-d_8 were treated with NaBAr$^F_4$ (Ar^F = 3,5-bis(trifluoromethyl)phenyl) as a chloride abstracting reagent. Characterization of the resulting crude mixture by NMR spectroscopy and high-resolution mass spectrometry (HRMS) gave evidence for formation of an N_2-bridged complex, [(PONOP)ReCl$_2$]$_2$(μ-N_2), but the reaction was slow and the yield was poor (approximately 30% yield after 75 h). An improved synthesis was achieved through direct treatment of the neutral complex **1** with 1 equiv of LiHBEt$_3$ in toluene under 1 atm N_2 at room temperature (Scheme 2).[41] After 40 min, the N_2-bridged complex was isolated in 53% yield (92% purity, with the remaining 8% a closely related species, *vide infra*). An XRD study revealed a *trans* configuration of the chloride ligands on each metal, [*trans*-(PONOP)Re^{II}Cl$_2$]$_2$(μ-N_2) ($\mathbf{3^{t,t}}$, Scheme 2 and Figure 3E). The planes defined by the pincer ligands in $\mathbf{3^{t,t}}$ are nearly orthogonal, imparting pseudo-D_{2d} symmetry. The frequency of the NN stretching vibration of $\mathbf{3^{t,t}}$ was determined to be 1776 cm^{-1} using solid-state resonance Raman spectroscopy (633 nm excitation). Sharp, paramagnetically shifted ^{1}H and ^{31}P NMR signals suggested an even-electron species with TIP, similar to other d^5-d^5 μ-N_2 Re complexes.[30,42]

In an attempt to trigger N≡N bond scission, complex $\mathbf{3^{t,t}}$ was heated at 130 °C in toluene-d_8 (Figure 3A). There was no indication of nitride formation, but the minor species present in samples of $\mathbf{3^{t,t}}$ (*vide supra*) became more prominent within minutes of heating and was joined by a new species upon prolonged heating (Figure 3B,C). The observed species are assigned as the isomeric N_2-bridged dirhenium complexes [*trans*-(PONOP)Re^{II}Cl$_2$](μ-N_2)[*cis*-(PONOP)Re^{II}Cl$_2$] ($\mathbf{3^{t,c}}$) and [*cis*-(PONOP)Re^{II}Cl$_2$]$_2$(μ-N_2) ($\mathbf{3^{c,c}}$), on the basis of NMR experiments including ^{1}H, ^{31}P{^{1}H}, ^{1}H-^{1}H COSY, and ^{1}H-^{31}P HMBC. In addition, DOSY NMR experiments indicated dimeric structures for all of these complexes, based on their smaller diffusion coefficients than **1** as a monomeric internal standard (Figure 3D).

Scheme 3. (A) Relative energy of the isomers of ^{3}**3**, in the triplet ground state, and the activation and reaction energy of thermal μ-N_2 cleavage. Computed N_2 cleavage transition states take on a zigzag geometry, with **TS-3^{t,c}** depicted as a representative example. (B) Free energy diagram for N_2 association to **2**. A transition state was identified for *cis* addition (**TS-i2^{c}**); a flat potential energy surface required the Re–N_2 distance in **TS-i2^{t}** to be fixed at 2.88 Å. In kcal/mol; computed at the M06L/def2 level in toluene continuum at 298 K. See SI Section XVI for more details.

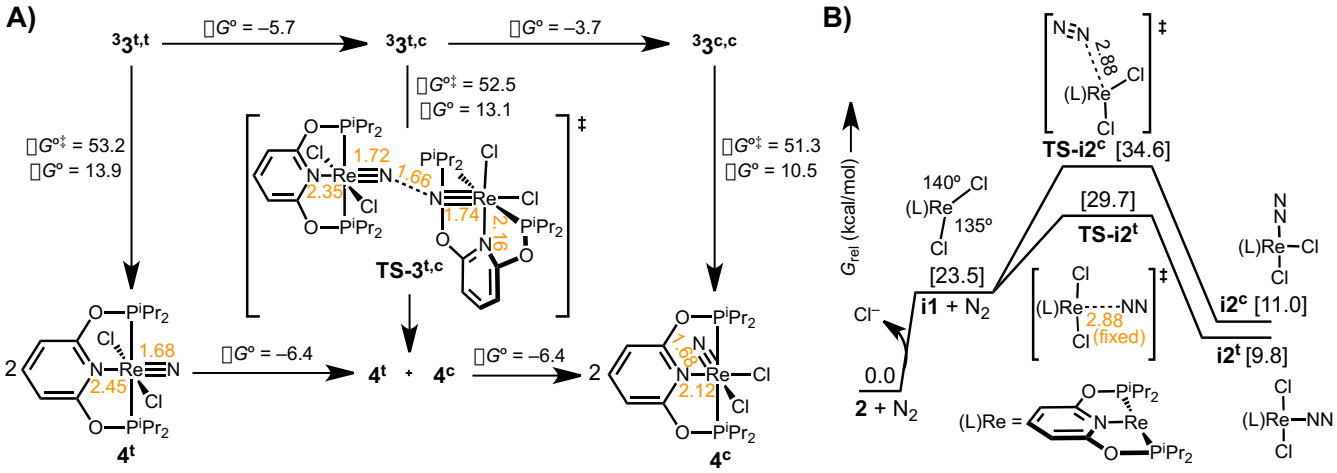

The time course of Figure 3B is consistent with sequential isomerization of **3^{t,t}** to **3^{t,c}** and then to **3^{c,c}** (Figure 3A). While prolonged heating over 3 days resulted in decomposition to predominantly **1** (47% yield, >44% unaccounted mass balance), thermolysis for 1.5 h enabled isolation of an approximately 1:1 mixture of **3^{t,c}** and **3^{c,c}** (98% pure, <2% impurity of **1**) on a preparative scale (26% overall yield). The solid-state resonance Raman spectrum (633 nm excitation) of the mixture further confirmed the presence of a bridging N_2 ligand, with a broad band centered at 1749 cm^{-1} assigned to the NN stretching vibration. An XRD analysis of the dark green crystals that grew upon slow evaporation of an Et_2O solution of the thermolysis products confirmed the structure of **3^{t,c}** (Figure 3F).

Thermal isomerization reactions of N_2-bridged species are rare,[22,43,44] so we sought to explore the different properties and reactivity of the isomers of **3**. The NMR time course suggests that the relative free energies of the N_2-bridged complexes favor **3^{t,t}** < **3^{t,c}** < **3^{c,c}**. DFT calculations show **3^{t,c}** to be more stable than **3^{t,t}** (ΔG° = –5.7 kcal/mol) and **3^{c,c}** more stable than **3^{t,c}** (ΔG° = –3.7 kcal/mol) (Scheme 3A), which is consistent with the experimental isomerization data. If complex **3^{t,t}** is the least stable isomer, its initial isolation must therefore be the result of a kinetic preference for a *trans*-dichloride orientation.

The kinetic preference for formation of **3^{t,t}** from **2** was investigated using DFT calculations (Scheme 3B). Chloride loss from **2** to generate the five-coordinate intermediate **i1** was calculated to be endergonic, consistent with the need for addition of Na^+ to drive this process experimentally. The distorted trigonal bipyramidal intermediate **i1** features an acute N–Re–Cl angle of 85°and a SOMO predominantly comprised of a Re d_{z2} AO that is aligned between the two chloride ligands (Figure S97).

The activation barriers of N_2 association along different trajectories of approach to **i1** determine the stereochemistry of the resulting *cis* or *trans* octahedral dichloride dinitrogen complex (**i2^{c}** and **i2^{t}** in Scheme 3B). N_2 approach perpendicular to the plane of the pincer would produce **i2^{c}**, while approach between the two chlorides would give **i2^{t}**. There is only a small thermodynamic preference for **i2^{t}**, but the computed potential energy surfaces for N_2 coordination to **i1** support a large kinetic preference for formation of **i2^{t}** (see SI Section XVI). Intermediate **i1** can react with **i2^{t}** to produce the triplet spin states of either **3^{t,t}** ($\Delta G°$ = -22.2 kcal/mol) or **3^{t,c}** ($\Delta G°$ = –27.9 kcal/mol). Low barriers for formation of either **3^{t,t}** or **3^{t,c}** are indicated by flat potential energy surfaces that lack transition states along either reaction coordinate (see SI Section XVI). These results predict that only **3^{t,t}** and **3^{t,c}** should be formed at room temperature, matching experimental observations.

Experimental support for an isomerization mechanism involving fragmentation of Re–N_2 bonds was obtained in a labeling study. Heating **3^{t,t}** at 120 °C for 1 h in toluene-d_8 under 1 atm $^{15}N_2$ resulted in the formation of two isotopologues by $^{31}P\{^{1}H\}$ NMR spectroscopy (Figure S82), assigned as **3^{t,t}($^{15}N_2$)** and **3^{t,c}($^{15}N_2$)**. Formation of these isotopologues requires Re–N_2 bond cleavage, suggesting that dimer dissociation to **i1** and **i2^{t}** precedes isomerization ($\Delta G°_{diss}$ = 22.2 kcal/mol based on unadjusted entropies, see SI Section XVI).[45]

To understand why N_2 splitting did not occur upon heating, we investigated the reaction using DFT methods. For all isomers of **3**, the thermodynamics of N_2 cleavage into the corresponding isomeric nitride products *trans*-(PONOP)Re(N)Cl_2 (**4^{t}**) and *cis*-(PONOP)Re(N)Cl_2 (**4^{c}**) was significantly endergonic, $\Delta G°$ = +10.5 to +13.9 kcal/mol (in toluene continuum, Scheme 3A).[46] One explanation for the unfavorable thermodynamics is the octahedral geometry, which destabilizes the product due to the strong *trans* influence of the nitride ligand.[47] DFT studies support this notion, with N_2 cleavage becoming thermodynamically more favorable upon sequential removal of each chloride ligand *trans* to the ReNNRe core of **3** (see SI Section XVI). This computational observation suggests that the relatively weak donating ability of the PONOP pincer ligand is not an impediment to N_2 splitting,

but rather that the presence of a ligand *trans* to the N_2 bridge is the dominant factor.

In addition, the calculations predict prohibitively high kinetic barriers for thermal N_2 cleavage for all isomers of **3**, $\Delta G^{\ddagger}$ = 51 – 53 kcal/mol (Scheme 3). Although terminal nitride **4** dimerizing to **3** is computed to be exergonic by about 10 kcal/mol, the thermal kinetic barrier of nitride coupling remains high, ca. 40 kcal/mol. Each transition state (TS) structure takes on the "zigzag" geometry generally observed in such reactions,[42,48] with substantial lengthening of the NN bond and contraction of the ReN bond (the TS associated with cleavage of $\mathbf{3^{t,c}}$ is included in Scheme 3 as a representative example). The product-like "zigzag" TS structures are destabilized by the octahedral geometry for the same reasons the nitride product itself is destabilized.[48] Lower kinetic barriers for N_2 cleavage by $\mathbf{3^{t,t}}$ are computed when one ($\Delta G^{\ddagger}$ = 35.4 kcal/mol) or two ($\Delta G^{\ddagger}$ = 21.0 kcal/mol) vacant sites are introduced *trans* to the ReNNRe core by chloride removal (see SI Section XVI).

Considering that N_2 cleavage in **3** is endergonic, the nitride products **4** might be formed reversibly. The kinetic accessibility of N_2 splitting was probed via thermal isomerization of an approximately 1:1 mixtures of $\mathbf{3^{t,t}}$ and $\mathbf{3^{t,t}(^{15}N_2)}$ at 130 °C for 1 h under an Ar atmosphere. NMR and HRMS analysis after heating revealed no evidence of the isotopologue **3(**^{14}**N**^{15}**N)**, the product that would result from isotopic scrambling during reversible N_2 splitting.

The lack of thermal N_2 splitting was surprising in the context of related systems, because each isomer of **3** was expected to have an electronic structure similar to (pincer)Mo and (pincer)Re complexes that thermally cleave N_2 at or below ambient temperature.[13,16,29] In seminal work investigating d^3 (Ar(^{t}Bu)N)$_3$Mo complexes, Cummins proposed a thermodynamic model based on the availability of 10 π-electrons, which would result in maximal stability of the triply-bonded nitride product.[48–50] This π^{10} model has subsequently correlated with N_2 cleavage in d^5 pincer complexes.[26,27,29,51] Isomers of **3** satisfy this π^{10} model, and yet are thermally stable. A similar situation was encountered for the thermally stable octahedral complex [*trans*-(HPNP^{iPr})ReCl$_2$]$_2$(μ-N$_2$).[30]

Our computational and experimental data suggest that coordinative unsaturation — in particular the presence of a vacant site *trans* to the MNNM core — is necessary for kinetically facile and thermodynamically favorable N_2 splitting.

2.2 Photolytic Reactivity of Bridging N_2 Isomers. With thermal N_2 cleavage inaccessible, photolytic cleavage of N_2 was explored, leveraging a unique opportunity to compare the reactivity of a series of isomeric bridging N_2 complexes.

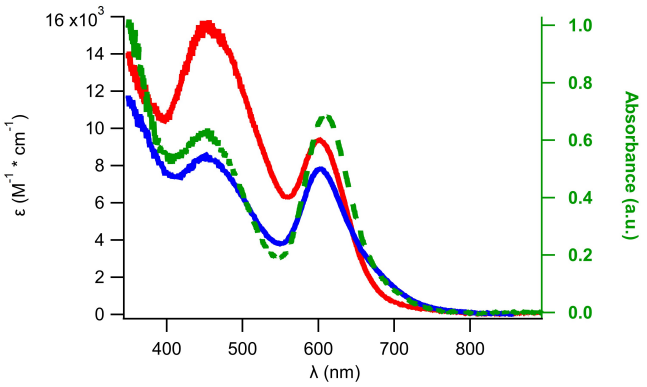

Figure 4. Electronic absorption spectra of $\mathbf{3^{t,t}}$ (solid red line, λ_{max} = 456 nm, ε = 16,000 $M^{-1}\cdot cm^{-1}$; λ_{max} = 601 nm, ε = 9,400 $M^{-1}\cdot cm^{-1}$; >8:1 ratio of $\mathbf{3^{t,t}}$:$\mathbf{3^{t,c}}$), $\mathbf{3^{t,c}}$ (solid blue line, λ_{max} = 452 nm, ε = 8600 $M^{-1}\cdot cm^{-1}$; λ_{max} = 604 nm, ε = 7,800 $M^{-1}\cdot cm^{-1}$; >7:1 ratio of $\mathbf{3^{t,c}}$:$\mathbf{3^{c,c}}$), and an approximately 1:1 $\mathbf{3^{t,c}}$:$\mathbf{3^{c,c}}$ mixture (dashed green line, λ_{max} = 453 nm and 610 nm) in THF.

Electronic absorption spectra of $\mathbf{3^{t,t}}$, $\mathbf{3^{t,c}}$, and a 1:1 mixture of $\mathbf{3^{t,c}}$:$\mathbf{3^{c,c}}$ all feature two intense bands in the visible region (Figure 4). Illumination of a saturated toluene-d_8 solution of primarily $\mathbf{3^{t,t}}$ (8:1 ratio of $\mathbf{3^{t,t}}$:$\mathbf{3^{t,c}}$) with blue light (405 nm LED) resulted in slow consumption of **3** over 9 days. The photolysis generated **1** as well as NMR silent products with only trace conversion to a single diamagnetic product. This minor diamagnetic product was confirmed to be the terminal nitride complex *cis*-(PONOP)Re^{V}(N)Cl$_2$ ($\mathbf{4^c}$, Figure 5) by comparison to an independently synthesized sample. Single crystal XRD confirmed the *cis* configuration of the chloride ligands. The strong *trans* influence of the nitride ligand is evident in a 0.2 Å elongation of Re–Cl2 relative to Re–Cl1.

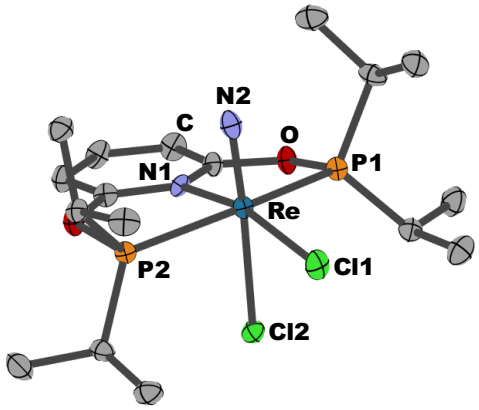

Figure 5. Structural representation of $\mathbf{4^c}$ derived from X-ray diffraction analysis. See SI Section VIII for bond lengths and angles.

Surprisingly, the *trans,cis* and *cis,cis* isomers of **3** showed a much greater photoreactivity. Starting with a saturated toluene-d_8 solution of $\mathbf{3^{t,c}}$ and $\mathbf{3^{c,c}}$ in a 1:1.3 ratio, illumination using a 405 nm LED resulted in 47% ± 3% NMR spectroscopic yield of $\mathbf{4^c}$ (average of three runs, moles of $\mathbf{4^c}$ divided by total moles of Re in the $\mathbf{3^{t,c}}$/$\mathbf{3^{c,c}}$ mixture) after approximately 7 h. The photochemical

quantum yield, defined as the moles of **4**^{c} per photon absorbed by the **3**^{t,c}/**3**^{c,c} mixture at early reaction times (see SI Section XIII), was approximated, $\Phi = 0.11 \pm 0.01$ at 2 h (Scheme 4). Similar chemical yields and quantum yields were observed at the standard LED current of 1000 mA and at lower current (500 mA). Photolysis of a $^{15}N_2$-enriched sample of **3**^{t,c}:**3**^{t,c} resulted in formation of **4**^{c}**(**^{15}**N)**, which gave a diagnostic nitrido ^{15}N resonance at δ 410.5 ppm, confirming that the observed nitride ligand originates from the bridging N_2.[30,31] Illumination of the **3**^{t,c}:**3**^{c,c} mixture using 455 nm LED resulted in slower conversion to **4**^{c} (47% yield in 1.5 days, $\Phi = 0.004$ at 1 h), whereas illumination with either 505 or 625 nm LED lamps for 24 h did not produce any detectable nitride products.

Scheme 4. Photolytic N_2 Cleavage of **3** to **4**^{c}. Isomeric ratios and yields were measured by ^{1}H NMR spectroscopy.

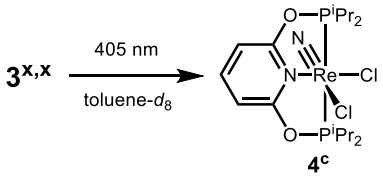

Isomeric Ratio			Φ	Yield	Time
3^{t,t}	**3**^{t,c}	**3**^{c,c}	(@ 2 h)		
8	1	0	0.003	< 3%	> 9 days
0	7	1	0.06	24%	7.5 h
0	1	1	0.12	51%	7 h

Isomer-specific photocleavage was further studied by examining dimer mixtures enriched in **3**^{t,c} *via* crystallization. Photolysis of a 7:1 mixture of **3**^{t,c}:**3**^{c,c} in toluene-d_8 resulted in decreased yields of **4**^{c} (24% yield, $\Phi = 0.06$ at 2 h, Scheme 4). Thus, **3**^{c,c} has by far the highest photoactivity in N_2 cleavage. In comparison, the *trans,trans* isomer **3**^{t,t} appears to be inert; the trace amounts of **4**^{c} observed upon photolysis of 8:1 **3**^{t,t}:**3**^{t,c} can be attributed entirely to photolysis of **3**^{t,c}.

The cleavage of **3**^{c,c} to form nitride **4**^{c} is computed to be endergonic by 10.5 kcal/mol (*vide supra*). However, no reversion of **4**^{c} back to N_2-bridged species by N–N coupling was observed even after prolonged heating in toluene solutions at 120 ºC or after photolysis with a 405 nm LED at 25 ºC (SI Section XII). This is consistent with the high kinetic barrier computed for thermal N_2 splitting/coupling. The high thermal barrier arising from coordinative saturation in the PONOP complexes thus plays a key role in enabling the successful photochemical reaction by preventing the thermal decomposition of **4**^{c} back to **3**.

Photochemical N_2 splitting to terminal nitrides remains a relatively rare transformation,[52] with only a handful of examples at Mo,[25,28,50] Re,[30] and Os.[53] The reaction often requires high energy light ($\lambda < 400$ nm).[28,53] Some examples report wavelength-dependent reactivity[25,30] similar to that observed for **3**, implicating a direct role for a high energy excited state. All Mo and Re examples of photochemical N_2 cleavage have an appropriate π^{10} electron configuration to maximize π-bonding in the nitride product.[25,28,30,50] The importance of an appropriate electron configuration is apparent in a recent study of d^5 [(depf)Mo(Cp*)]$_2$(μ-N_2) (depf = bis(diethylphosphino)ferrocene), which has a π^{10} configuration and photochemically splits N_2, whereas the singly or doubly oxidized congeners (π^9 or π^8, respectively) are photochemically inert.[25]

Until now, no comparative study of geometric isomers undergoing photolytic N_2 cleavage has been reported. We find that each isomer exhibits markedly different photoreactivity. The isomer **3**^{t,t} produces essentially no nitride product, while the thermodynamically most stable isomer **3**^{c,c} exhibits the highest quantum efficiency and highest yield of nitride complex. The poor photochemical activity of **3**^{t,t} is surprising because the structurally analogous complex [*trans*-(HPNP^{iPr})ReCl$_2$]$_2$(μ-N_2) *does* photolytically cleave N_2 using violet light (390 nm) to exclusively yield *cis*-(HPNP^{iPr})Re(N)Cl$_2$, with no evidence of a *trans*-(HPNP^{iPr})Re(N)Cl$_2$ product.[30] The isomer-specific reactivity observed in our study suggests that future catalyst candidates should be designed with geometric considerations in mind.

2.3 PCET Nitride Reduction to Ammonia. The feasibility of various proton-coupled electron transfer (PCET) routes from the N_2-derived nitride **4**^{c} to NH_3 were initially explored using DFT methods. As shown in Scheme 5, the stepwise pathway initiated by proton transfer (PT) would require very strong acids ($pK_a \sim -2.4$ in THF), while the pathway initiated by electron transfer (ET) would require strongly reducing conditions. The computed pK_a and $E°$ values were used to calculate the bond dissociation free energy (BDFE) of the parent imido complex, BDFE = 43 kcal/mol (Scheme 5; an independent BDFE computation based on the free energy of HAT from TEMPOH to **4**^{c} gave a value of 42 kcal/mol).[54]

Scheme 5. Computed PCET square scheme of **4**^{c} in THF.[a] See SI Section XVI for more details.

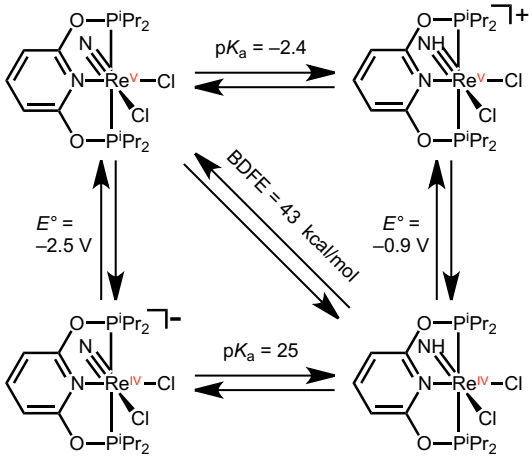

[a] $E°$ is computed versus a $CoCp^*_2$ reference, values are reported versus $Fc^{+/0}$. pK_a is computed versus a pyridinium reference, reported on the THF pK_a scale. BDFE is calculated from these values and averaged using $BDFE = 1.37(pK_a) + 23.06(E°) + C_G$ (C_G for THF = 66 kcal/mol).[55]

Experiments also indicated that stepwise pathways would be challenging. CV experiments of **4**^{c} in THF revealed two irreversible reductions (E_{pc} = –2.38 and –2.63 V vs. $Fc^{+/0}$),

indicating rapid chemical steps following reduction. Attempts at protonation of **4**^{c} using up to 100 equiv HCl (2.0 M in Et_2O, pK_a = 10 in THF)[56,57] in THF-d_8 resulted in no observable reaction over at least 1 h, providing experimental evidence for the low pK_a of the protonated nitride (Scheme 5, top).

To reach a parent imido intermediate with a weak N–H BDFE of 43 kcal/mol would require a strong acid and strong reductant, posing a challenge in reagent compatibility.[58] Instead, we sought a single, stable reagent capable of delivering a proton and an electron, perhaps even in a concerted fashion.[54,58] SmI_2/H_2O was identified as a promising candidate on the basis of its exceptionally low O–H BDFE (26 kcal/mol in H_2O) and its stability with respect to H_2 release.[59] The Sm^{II} aquo complex can also deliver H^+ and e^- equivalents to organic substrates in a concerted fashion.[59–64] During preparation of this manuscript, two reports using SmI_2 to drive catalytic N_2 fixation at Mo were published.[15,65]

Treating **4**^{c} with 10 equiv of SmI_2 and 100 equiv H_2O in THF-d_8 resulted in a rapid reaction and the appearance of a broad 1:1:1 triplet in the ^{1}H NMR spectrum (7.14 ppm, J_{HN} = 48.6 Hz) characteristic of NH_4^+ (Scheme 6). The production of NH_4^+ was confirmed by ion chromatography (IC, 74% ± 3%, average of three trials)[66,67] and ^{1}H NMR spectroscopy (77% ± 9% yield, average of three trials). Along with NH_4^+, one new dominant diamagnetic product was observed by ^{31}P NMR spectroscopy (δ 208.9, 38% yield). 2D ^{1}H–^{31}P HMBC, selectively coupled ^{31}P NMR, and mass spectroscopy enabled assignment as (PONOP)Re(I)H_4, especially the observation of a quintet for the proton-coupled phosphorus resonance (Figure S78).[68] However, the instability of the Re product to vacuum prevented its isolation. It is noteworthy that the PONOP ligand successfully withstands the acidic conditions of NH_4^+ formation via SmI_2/H_2O reduction, remaining intact as a rhenium tetrahydride complex.

Scheme 6. SmI_2/H_2O PCET Reduction of **4**^{c} in THF.

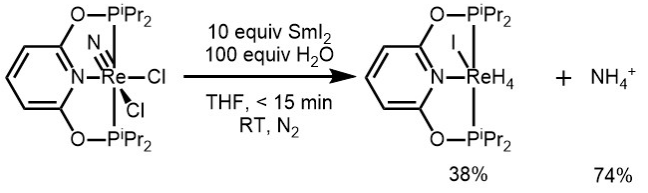

The presence of SmI_2 is essential for ammonia formation. Treating **4**^{c} with 30 equiv of H_2O (and no SmI_2) resulted in complete decomposition over 5 h with no detectable NH_4^+. Treating **4**^{c} with LaI_3 and 45 equiv H_2O resulted in some chloride-iodide exchange but produced <1% NH_4^+. Including the Lewis acid did result in prolonged water stability (only ~20% had decomposed after 48 h). Additionally, the use of the nitride-containing **4**^{c} is equally important. Treatment of **1** with 10 equiv of SmI_2 and 100 equiv of H_2O in THF-d_8 resulted in < 3% yield of NH_4^+ concomitant with 50% yield of the same (PONOP)Re(I)H_4 product.

To confirm that the NH_4^+ was derived from N_2, a streamlined one-pot N_2 fixation sequence was developed. A Teflon-sealed NMR tube was charged with a toluene-d_8 solution of the **3**^{t,t} and heated at 130 °C under $^{15}N_2$ (1 atm at ambient temperatures) for 60 min, resulting in a mixture of N_2-bridged isomers **3**^{t,c} and **3**^{c,c} with significant $^{15}N_2$-enrichment (See S95). Photolysis at 405 nm for 24 h yielded 24% of a mixture of **4**^{c} and the labeled nitride, **4**^{c}**(**^{15}**N)**. The solvent was removed and the residual solids were dissolved in THF-d_8, to which 100 equiv of H_2O then 10 equiv of solid SmI_2 were consecutively added. Free $^{15}NH_4^+$ was detected by ^{15}N{^{1}H} (–351 ppm) and ^{1}H NMR spectroscopy (7.29 ppm, d, J_{HN} = 72.6 Hz), with 33% yield quantified by IC relative to **4**^{c}**(**^{15}**N)** (8% overall yield from **3**^{t,t}). This series of reactions confirms that N_2 can be converted to NH_4^+ at rhenium via well-characterized initial N≡N bond scission.

The use of SmI_2/H_2O, which can provide both H^+ and e^-, proved much more successful for nitride reduction as compared to attempts at stepwise protonation and reduction. We therefore explored the use of other O–H and C–H PCET reagents under conditions analogous to those described above (10 equiv, room temperature). Treating nitride complex **4**^{c} with 2,4,6-tri-tertbutylphenol (O–H BDFE = 77 kcal/mol in MeCN)[54], TEMPOH (O–H BDFE = 67 kcal/mol in MeCN)[54], or 1,8-dichloro-9,10-dihydroxyanthracene (average O–H BDFE = 60 kcal/mol in H_2O)[69] resulted in no reactivity over 1 h. The lack of observed reactivity is consistent with a lack of driving force for N–H bond formation using these reagents, which have stronger O–H bonds compared to SmI_2/H_2O (BDFE = 26 kcal/mol in H_2O).[59] In contrast, treating **4**^{c} with $CoCp_2^*$ and $Ph_2NH_2^+$ produces NH_4^+ in 24% yield. These conditions can generate [Co(Cp*)(Cp*H)] (C–H BDFE < 29 kcal/mol in butyronitrile),[37,70,71] which features a C–H BDFE similar to the O–H BDFE of SmI_2/H_2O.

Formation of ammonia from nitride complex **4**^{c} was only observed using species with exceptionally weak BDFE values that provide at least –14 kcal/mol of thermodynamic driving force for initial N–H bond formation. The first N–H bond formation is often proposed to be the most difficult of the imide/amide/ammine series,[72,73] and the same trend is predicted computationally in the present system (see SI Section XVI). In accord with this trend, the driving force for delivery of the *second* H^+/e^- equivalent was calculated to be quite large (~–52 kcal/mol, see SI Section XVI), implicating rapid formation of the more stable amido species. The utility of SmI_2/H_2O, in particular, is rapidly becoming clear, with recent examples of catalytic N_2 fixation by Mo complexes and the present example of ammonia synthesis facilitated by a Re complex.[15,65]

2.4 Insight into Key Steps in the Reduction of N_2 to NH_3. The ability to isolate many intermediates along the pathway from N_2 to NH_3 provides an opportunity to assess the molecular features that drive the individual steps in this process. The broad implications of reductive binding of N_2, thermal N_2 splitting, photochemical N_2 splitting, and initial N–H bond formation are discussed here.

Reduction of metal halide complexes is typically proposed as the initial step along N_2 activation pathways. An ideal electrocatalyst undergoes reduction at mild potentials followed by rapid halide dissociation and N_2 binding. The electrochemical properties of (PONOP)$ReCl_3$ (**1**) can be compared with the previously studied complexes (HPNP^{iPr})$ReCl_3$ and (PNP^{tBu})$ReCl_2$

to assess the factors that influence reductive N_2 binding. Complex **1** is by far the easiest to reduce of the series (by approximately 600 mV). The relatively mild reduction potential of **1** reflects a less electron rich metal center relative to the trialkylphosphine-based systems. Probably due to the less electron-rich nature of **1**, chloride loss does not occur spontaneously after initial 1e– reduction; a vacant coordination site can be opened by halide abstraction with an alkali metal cation.[6] In contrast, (H-PNP^{iPr})ReCl$_3$ and (PNP^{tBu})ReCl$_2$ (k_{diss} = 1000 s^{-1}) both release chloride after reduction.[29,30] Steric bulk also plays a role in promoting halide dissociation,[42] and this may be a factor in systems with bulky phosphine substituents.

Although the present system binds N_2 to form an end-on-bridged dirhenium complex, thermal splitting to form a nitride complex is not observed. Qualitative molecular orbital diagrams have provided an intuitive view into the importance of maximizing π-bonding in the metal nitride bonds that form upon N_2 splitting.[27,48,50,51] However, despite an appropriate orbital configuration, thermal N_2 splitting from the isolated isomeric N_2-bridged complexes **3** is not observed. DFT computations suggest that the reaction is thermodynamically unfavorable (endergonic by at least 10 kcal/mol) and kinetically demanding (with barriers above 50 kcal/mol). Our observations provide additional evidence for a key role of coordination number in the thermodynamics and kinetics of N_2 cleavage. In particular, a vacant site *trans* to the N_2 bridge is critical. This is apparent in comparisons of both Re and Mo systems. Thermal cleavage is not observed by Schneider in six-coordinate Re systems, whereas rapid N_2 cleavage below room temperature is observed in a structurally similar coordinatively unsaturated complex.[29,30] Furthermore, Cummins' four-coordinate dimolybdenum(III) bridging N_2 complex with a *trans* vacant site spontaneously cleaves N_2, while Schrock's isoelectronic five-coordinate complex that positions an amine ligand *trans* to the bridging N_2 unit is thermally stable.[16,51,74] To our knowledge, *every example* of thermal N_2 splitting to a terminal nitride complex at or below ambient temperature features a coordinatively unsaturated N_2-bridged species.[13–16,23,26,27,29,41] These observations suggest that future systems should be designed to enforce coordination vacancies *trans* to the MNNM core when targeting N_2 splitting reactions with a low kinetic barrier.

The conversion of PONOP-supported N_2-bridged complex **3**^{c,c} to terminal nitride complex **4**^{c} proceeds under visible light illumination with high quantum efficiency. Interestingly, the *cis*,*cis* dimer exhibits by far the highest photochemical reactivity, suggesting that stereochemical control of the metal center may be critical in future systems. The N_2 splitting reaction is endergonic, with the product protected from reverting to N_2 by the high thermal NN splitting/coupling barrier. This free energy profile raises the possibility of designing systems that use photon energy to generate a higher energy nitride that might be more reactive in subsequent steps.

Nitride complexes derived from N_2 splitting have only rarely been converted to ammonia. For example, Holland and coworkers cleaved N_2 to form a bridging nitride diiron complex, then released ammonia by stepwise reduction and treatment with acids or H-atom donors.[12] Additionally, Nishibayashi recently showed that (pincer)Mo systems can reductively cleave N_2 to form a terminal nitride complex that releases NH_3 upon treatment with SmI_2 and water or alcohols.[15,65] The PONOP-supported system in focus here enabled the first example of ammonia formation from an N_2-derived rhenium nitride upon treatment with SmI_2/H_2O.

The use of reagents or conditions capable of providing H^+/e^- together has emerged as a broader theme in N_2 reduction research. Peters recently showed that metallocene/acid combinations can behave as PCET reagents,[37,70,71] and Chirik has recently demonstrated light-driven PCET reduction of a manganese nitride.[75,76] Thermochemical analyses underpin this approach,[77,78] as it can be critical to choose a reagent or conditions that provide ample driving force for both the first and second N–H bond formation. Tuning the reactivity towards exergonic N–H bond formation, and perhaps even towards concerted H^+/e^- transfer, could be important factors in achieving kinetically efficient nitride reduction to release ammonia as part of a catalytic or electrocatalytic system.

3. CONCLUSIONS

The multistep reduction of dinitrogen to ammonia has been facilitated by a molecular rhenium complex for the first time. Reduction of (PONOP)ReCl$_3$ led to formation of an N_2-bridged species that undergoes *cis*/*trans* isomerization at high temperatures. The thermal stability enabled a unique comparative study of photochemical N_2 splitting across three geometric isomers, with the *cis*,*cis* isomer exhibiting the highest photoreactivity. A computational thermochemical analysis of H^+/e^- addition guided the choice of SmI_2/H_2O for the reduction of the rhenium nitride, releasing ammonia in high yield.

The detailed characterization of many intermediates along the reaction pathway provides key insights into the factors that enable N_2 reduction to NH_3 via an N_2 splitting mechanism. (1) Ligand electronic structure can tune the reduction potential, with the PONOP ligand supporting mild reduction potentials compared to other (pincer)Re complexes. (2) Coordinatively unsaturated metal centers that enforce a vacant site *trans* to the site of N_2 activation lead to more exergonic N_2 splitting and lower the kinetic barrier for the reaction. (3) Photochemical N_2 splitting is viable at coordinatively saturated metal centers, and here we show that different geometric isomers in an isoelectronic series can have dramatically different quantum efficiencies for nitride formation. The high thermal kinetic barrier for N_2 splitting prevents the exergonic coupling to re-form the N_2-bridged species. (4) Ammonia formation from N_2-derived nitride ligands is typically challenging because of the weak BDFE of many metal imides (M=NH).[73,79] The use of potent H^+/e^- donors can provide access to this key intermediate on the path to ammonia. SmI_2/H_2O provides ample driving force for rapid N–H bond formation, while the protolytically stable PONOP ligand allows for well-defined reactivity at the desired position to release NH_4^+.

ASSOCIATED CONTENT

Supporting Information

Experimental details and characterization data (PDF)

Coordinates of optimized geometries in mol2 format, change extension to mol2 for visualization (TXT)
Crystallographic data (CIF)
This material is available free of charge via the Internet at http://pubs.acs.org.

AUTHOR INFORMATION

Corresponding Author

* F.H. Email: fh19@aub.edu.lb
* A.J.M.M. Email: ajmm@email.unc.edu

ACKNOWLEDGMENT

The experimental work was supported through the NSF Chemical Catalysis program under Grants No. CHE-1665135 and CHE-1665137. Q.J.B. acknowledges support from the NSF Graduate Research Fellowship Program (DGE-1650116). Support for computational studies was provided by a grant from LNCSR-AUB. The authors thank B. Ehrmann for assistance with mass spectrometry and ion chromatography, M. K. Brennaman for assistance with resonance Raman spectroscopy, C. Hartley for assistance with EPR spectroscopy, and M. ter Horst for assistance with selective coupling NMR experiments. The authors would also like to thank the high performance computing centers at American University of Beirut and Rutgers University for computational resources. The mass spectrometry work was supported by the National Science Foundation under Grant No. (CHE-1726291). A portion of this work was performed using the Renishaw inVia Raman microscope in the AMPED EFRC Instrumentation Facility established by the Alliance for Molecular PhotoElectrode Design for Solar Fuels, an Energy Frontier Research Center (EFRC) funded by the U.S. Department of Energy, Office of Science, Office of Basic Energy Sciences under Award DE-SC0001011.

REFERENCES

(1) Erisman, J. W.; Sutton, M. A.; Galloway, J.; Klimont, Z.; Winiwarter, W. How a Century of Ammonia Synthesis Changed the World. *Nat. Geosci.* **2008**, *1*, 636–639.

(2) Shipman, M. A.; Symes, M. D. Recent Progress towards the Electrosynthesis of Ammonia from Sustainable Resources. *Catal. Today* **2017**, *286*, 57–68.

(3) Chen, X.; Li, N.; Kong, Z.; Ong, W.; Zhao, X. Photocatalytic Fixation of Nitrogen to Ammonia: State-of-the-Art Advancements and Future Prospects. *Mater. Horizons* **2018**, *5*, 9–27.

(4) Liu, H.; Wei, L.; Liu, F.; Pei, Z.; Shi, J.; Wang, Z.; He, D.; Chen, Y. Homogeneous, Heterogeneous, and Biological Catalysts for Electrochemical N_2 Reduction toward NH_3 under Ambient Conditions. *ACS Catal.* **2019**, *9*, 5245–5267.

(5) Čorić, I.; Holland, P. L. Insight into the Iron–Molybdenum Cofactor of Nitrogenase from Synthetic Iron Complexes with Sulfur, Carbon, and Hydride Ligands. *J. Am. Chem. Soc.* **2016**, *138*, 7200–7211.

(6) Connor, G. P.; Holland, P. L. Coordination Chemistry Insights into the Role of Alkali Metal Promoters in Dinitrogen Reduction. *Catal. Today* **2017**, *286*, 21–40.

(7) Stucke, N.; Flöser, B. M.; Weyrich, T.; Tuczek, F. Nitrogen Fixation Catalyzed by Transition Metal Complexes: Recent Developments. *Eur. J. Inorg. Chem.* **2018**, *2018*, 1337–1355.

(8) Nishibayashi, Y. Development of Catalytic Nitrogen Fixation Using Transition Metal-Dinitrogen Complexes under Mild Reaction Conditions. *Dalt. Trans.* **2018**, *47*, 11290–11297.

(9) Chatt, J. A Possible Mimic of the Nitrogenase Reaction. In *Biomimetic Chemistry*; Dolphin, D., Mckenna, C., Murakami, Y., Tabushi, I., Eds.; American Chemical Society, 1980; pp 379–391.

(10) Yandulov, D. V; Schrock, R. R. Catalytic Reduction of Dinitrogen to Ammonia at a Single Molybdenum Center. *Acc. Chem. Res.* **2005**, *38*, 955–962.

(11) Rodriguez, M. M.; Bill, E.; Brennessel, W. W.; Holland, P. L. N_2 Reduction and Hydrogenation to Ammonia by a Molecular Iron-Potassium Complex. *Science* **2011**, *334*, 780–783.

(12) MacLeod, K. C.; McWilliams, S. F.; Mercado, B. Q.; Holland, P. L. Stepwise N–H Bond Formation from N_2-Derived Iron Nitride, Imide and Amide Intermediates to Ammonia. *Chem. Sci.* **2016**, *7*, 5736–5746.

(13) Arashiba, K.; Eizawa, A.; Tanaka, H.; Nakajima, K.; Yoshizawa, K.; Nishibayashi, Y. Catalytic Nitrogen Fixation via Direct Cleavage of Nitrogen-Nitrogen Triple Bond of Molecular Dinitrogen under Ambient Reaction Conditions. *Bull. Chem. Soc. Jpn.* **2017**, *90*, 1111–1118.

(14) Itabashi, T.; Mori, I.; Arashiba, K.; Eizawa, A.; Nakajima, K.; Nishibayashi, Y. Effect of Substituents on Molybdenum Triiodide Complexes Bearing PNP-Type Pincer Ligands toward Catalytic Nitrogen Fixation. *Dalt. Trans.* **2019**, *48*, 3182–3186.

(15) Ashida, Y.; Arashiba, K.; Nakajima, K.; Nishibayashi, Y. Molybdenum-Catalysed Ammonia Production with Samarium Diiodide and Alcohols or Water. *Nature* **2019**, *568*, 536–540.

(16) Laplaza, C. E.; Cummins, C. C. Dinitrogen Cleavage by a Three-Coordinate Molybdenum(III) Complex. *Science* **1995**, *268*, 861–863.

(17) Mena, M.; Pérez-Redondo, A.; Yélamos, C. Heterometallic Cube-Type Molecular Nitrides. *Eur. J. Inorg. Chem.* **2016**, *2016*, 1762–1778.

(18) Nikiforov, G. B.; Vidyaratne, I.; Gambarotta, S.; Korobkov, I. Titanium-Promoted Dinitrogen Cleavage, Partial Hydrogenation, and Silylation. *Angew. Chemie Int. Ed.* **2009**, *48*, 7415–7419.

(19) Bezdek, M. J.; Chirik, P. J. Expanding Boundaries: N_2 Cleavage and Functionalization beyond Early Transition Metals. *Angew. Chemie Int. Ed.* **2016**, *55*, 7892–7896.

(20) Gambarotta, S.; Scott, J. Multimetallic Cooperative Activation of N_2. *Angew. Chemie Int. Ed.* **2004**, *43*, 5298–5308.

(21) Shaver, M. P.; Fryzuk, M. D. Activation of Molecular Nitrogen: Coordination, Cleavage and Functionalization of N_2 Mediated By Metal Complexes. *Adv. Synth. Catal.* **2003**, *345*, 1061–1076.

(22) Chirik, P. J. Dinitrogen Functionalization with Bis(Cyclopentadienyl) Complexes of Zirconium and Hafnium. *Dalt. Trans.* **2007**, *127*, 16–25.

(23) Hebden, T. J.; Schrock, R. R.; Takase, M. K.; Müller, P. Cleavage of Dinitrogen to Yield a (t-BuPOCOP)Molybdenum(IV) Nitride. *Chem. Commun.* **2012**, *48*, 1851–1853.

(24) Liao, Q.; Cavaillé, A.; Saffon-Merceron, N.; Mézailles, N. Direct Synthesis of Silylamine from N_2 and a Silane: Mediated by a Tridentate Phosphine Molybdenum Fragment. *Angew. Chemie Int. Ed.* **2016**, *55*, 11212–11216.

(25) Miyazaki, T.; Tanaka, H.; Tanabe, Y.; Yuki, M.; Nakajima, K.; Yoshizawa, K.; Nishibayashi, Y. Cleavage and Formation of Molecular Dinitrogen in a Single System Assisted by Molybdenum Complexes Bearing Ferrocenyldiphosphine. *Angew. Chemie Int. Ed.* **2014**, *53*, 11488–11492.

(26) Silantyev, G. A.; Förster, M.; Schluschaß, B.; Abbenseth, J.; Würtele, C.; Volkmann, C.; Holthausen, M. C.; Schneider, S. Dinitrogen Splitting Coupled to Protonation. *Angew. Chemie Int. Ed.* **2017**, *56*, 5872–5876.

(27) Katayama, A.; Ohta, T.; Wasada-Tsutsui, Y.; Inomata, T.; Ozawa, T.; Ogura, T.; Masuda, H. Dinitrogen-Molybdenum Complex Induces Dinitrogen Cleavage by One-Electron Oxidation. *Angew. Chemie Int. Ed.* **2019**, *58*, 11279–11284.

(28) Solari, E.; Silva, C. Da; Iacono, B.; Hesschenbrouck, J.; Rizzoli, C.; Scopelliti, R.; Floriani, C. Photochemical Activation of the N≡N Bond in a Dimolybdenum-Dinitrogen Complex: Formation of a Molybdenum Nitride. *Angew. Chemie Int. Ed.* **2001**, *40*, 3907–3909.

(29) Klopsch, I.; Finger, M.; Würtele, C.; Milde, B.; Werz, D. B.; Schneider, S. Dinitrogen Splitting and Functionalization in the Coordination Sphere of Rhenium. *J. Am. Chem. Soc.* **2014**, *136*, 6881–6883.

(30) Schendzielorz, F.; Finger, M.; Abbenseth, J.; Würtele, C.; Krewald, V.; Schneider, S. Metal-Ligand Cooperative Synthesis of Benzonitrile by Electrochemical Reduction and Photolytic Splitting of Dinitrogen. *Angew. Chemie Int. Ed.* **2019**, *58*, 830–834.

(31) Klopsch, I.; Kinauer, M.; Finger, M.; Würtele, C.; Schneider, S. Conversion of Dinitrogen into Acetonitrile under Ambient Conditions. *Angew. Chemie Int. Ed.* **2016**, *55*, 4786–4789.

(32) Salem, H.; Shimon, L. J. W.; Diskin-Posner, Y.; Leitus, G.; Ben-David, Y.; Milstein, D. Formation of Stable *Trans* -Dihydride Ruthenium(II) and 16-Electron Ruthenium(0) Complexes Based on Phosphinite PONOP Pincer Ligands. Reactivity toward Water and Electrophiles. *Organometallics* **2009**, *28*, 4791–4806.

(33) Bernskoetter, W. H.; Hanson, S. K.; Buzak, S. K.; Davis, Z.; White, P. S.; Swartz, R.; Goldberg, K. I.; Brookhart, M. Investigations of Iridium-Mediated Reversible C−H Bond Cleavage: Characterization of a 16-Electron Iridium(III) Methyl Hydride Complex. *J. Am. Chem. Soc.* **2009**, *131*, 8603–8613.

(34) Espada, M. F.; Bennaamane, S.; Liao, Q.; Saffon-Merceron, N.; Massou, S.; Clot, E.; Nebra, N.; Fustier-Boutignon, M.; Mézailles, N. Room-Temperature Functionalization of N_2 to Borylamine at a Molybdenum Complex. *Angew. Chemie Int. Ed.* **2018**, *57*, 12865–12868.

(35) Pearson, C.; Beauchamp, A. ^{1}H NMR Study of Monomeric Chloro-Rhenium(III) Complexes with Triarylphosphines and Nitriles. *Inorg. Chim. Acta* **1995**, *237*, 13–18.

(36) Chatt, J.; Leigh, G. J.; Mingos, D. M. P. Configurations of Some Complexes of Rhenium, Ruthenium, Osmium, Rhodium, Iridium, and Platinum Halides with Mono(Tertiary Phosphines) and Mono(Tertiary Arsines). *J. Chem. Soc. A* **1969**, 1674.

(37) Chalkley, M. J.; Del Castillo, T. J.; Matson, B. D.; Roddy, J. P.; Peters, J. C. Catalytic N_2-to-NH_3 Conversion by Fe at Lower Driving Force: A Proposed Role for Metallocene-Mediated PCET. *ACS Cent. Sci.* **2017**, *3*, 217–223.

(38) Connelly, N. G.; Geiger, W. E. Chemical Redox Agents for Organometallic Chemistry. *Chem. Rev.* **1996**, *96*, 877–910.

(39) Boreen, M. A.; Lohrey, T. D.; Rao, G.; Britt, R. D.; Maron, L.; Arnold, J. A Uranium Tri-Rhenium Triple Inverse Sandwich Compound. *J. Am. Chem. Soc.* **2019**, *141*, 5144–5148.

(40) Mallick, S.; Ghosh, M. K.; Mandal, S.; Rane, V.; Kadam, R.; Chatterjee, A.; Bhattacharyya, A.; Chattopadhyay, S. The First Examples of Multiply Bonded Dirhenium(III,II) Paramagnetic Complexes Containing Nitrobenzoate Ligands: Spectroscopic, Structural, Cytotoxicity and Computational Studies. *Dalt. Trans.* **2017**, *46*, 5670–5679.

(41) Liao, Q.; Cavaillé, A.; Saffon-Merceron, N.; Mézailles, N. Direct Synthesis of Silylamine from N_2 and a Silane: Mediated by a Tridentate Phosphine Molybdenum Fragment. *Angew. Chemie Int. Ed.* **2016**, *55*, 11212–11216.

(42) Lindley, B. M.; Van Alten, R. S.; Finger, M.; Schendzielorz, F.; Würtele, C.; Miller, A. J. M.; Siewert, I.; Schneider, S. Mechanism of Chemical and Electrochemical N_2 Splitting by a Rhenium Pincer Complex. *J. Am. Chem. Soc.* **2018**, *140*, 7922–7935.

(43) Keane, A. J.; Yonke, B. L.; Hirotsu, M.; Zavalij, P. Y.; Sita, L. R. Fine-Tuning the Energy Barrier for Metal-Mediated Dinitrogen N≡N Bond Cleavage. *J. Am. Chem. Soc.* **2014**, *136*, 9906–9909.

(44) Bennett, M. A.; Byrnes, M. J.; Chung, G.; Edwards, A. J.; Willis, A. C. Bis(Acetylacetonato)Ruthenium(II) Complexes Containing Bulky Tertiary Phosphines. Formation and Redox Behaviour of $Ru(Acac)_2$ (PR_3)

(R = IPr, Cy) Complexes with Ethene, Carbon Monoxide, and Bridging Dinitrogen. *Inorg. Chim. Acta* **2005**, *358*, 1692–1708.

(45) The given $\Delta G°_{diss}$ value uses unscaled gas phase entropies computed at 298 K ($\Delta S°_{diss}$ = 59.6 cal·mol^{-1}·K^{-1}). Scaling the entropies by a factor of 0.5 affords $\Delta G°$diss = 31.1 kcal·mol^{-1} at 298 K, or 28.0 kcal·mol^{-1} at 403 K (the temperature of the experiment).

(46) The given $\Delta G°_{diss}$ values use unscaled gas phase entropies computed at 298 K ($\Delta S°_{diss}$ ≈ 58 cal·mol^{-1}·K^{-1}). Scaling the entropies by a factor of 0.5 affords $\Delta G°_{diss}$ = 18.8 – 22.9 kcal·mol^{-1} at 298 K, or 15.8 – 19.6 kcal·mol^{-1} at 403 K. The computed activation free energies of cleavage are insensitive to the entropy scaling factor and the temperature.

(47) Coe, B. J.; Glenwright, S. J. Trans-Effects in Octahedral Transition Metal Complexes. *Coord. Chem. Rev.* **2000**, *203*, 5–80.

(48) Laplaza, C. E.; Johnson, M. J. A.; Peters, J. C.; Odom, A. L.; Kim, E.; Cummins, C. C.; George, G. N.; Pickering, I. J. Dinitrogen Cleavage by Three-Coordinate Molybdenum(III) Complexes: Mechanistic and Structural Data. *J. Am. Chem. Soc.* **1996**, *118*, 8623–8638.

(49) Treitel, I. M.; Flood, M. T.; Marsh, R. E.; Gray, H. B. Molecular and Electronic Structure of μ-Nitrogen-Decaamminediruthenium(II). *J. Am. Chem. Soc.* **1969**, *91*, 6512–6513.

(50) Curley, J. J.; Cook, T. R.; Reece, S. Y.; Müller, P.; Cummins, C. C. Shining Light on Dinitrogen Cleavage: Structural Features, Redox Chemistry, and Photochemistry of the Key Intermediate Bridging Dinitrogen Complex. *J. Am. Chem. Soc.* **2008**, *130*, 9394–9405.

(51) Klopsch, I.; Yuzik-Klimova, E. Y.; Schneider, S. Functionalization of N_2 by Mid to Late Transition Metals via N–N Bond Cleavage. In *Topics in Organometallic Chemistry*; Nishibayashi, Y., Ed.; Springer, Cham, 2017; Vol. 60, pp 71–112.

(52) Rebreyend, C.; de Bruin, B. Photolytic N_2 Splitting: A Road to Sustainable NH_3 Production? *Angew. Chemie Int. Ed.* **2015**, *54*, 42–44.

(53) Kunkely, H.; Vogler, A. Photolysis of Aqueous $[(NH_3)_5Os(\mu\text{-}N_2)Os(NH_3)_5]^{5+}$: Cleavage of Dinitrogen by an Intramolecular Photoredox Reaction. *Angew. Chemie Int. Ed.* **2010**, *49*, 1591–1593.

(54) Warren, J. J.; Tronic, T. A.; Mayer, J. M. Thermochemistry of Proton-Coupled Electron Transfer Reagents and Its Implications. *Chem. Rev.* **2010**, *110*, 6961–7001.

(55) Cappellani, E. P.; Drouin, S. D.; Jia, G.; Maltby, P. A.; Morris, R. H.; Schweitzer, C. T. Effect of the Ligand and Metal on the pK_a Values of the Dihydrogen Ligand in the Series of Complexes $[M(H_2)H(L)_2]$+, M = Fe, Ru, Os, Containing Isosteric Ditertiaryphosphine Ligands, L. *J. Am. Chem. Soc.* **1994**, *116*, 3375–3388.

(56) Abdur-Rashid, K.; Fong, T. P.; Greaves, B.; Gusev, D. G.; Hinman, J. G.; Landau, S. E.; Lough, A. J.; Morris, R. H. An Acidity Scale for Phosphorus-Containing Compounds Including Metal Hydrides and Dihydrogen Complexes in THF: Toward the Unification of Acidity Scales. *J. Am. Chem. Soc.* **2000**, *122*, 9155–9171.

(57) Morris, R. H. Brønsted–Lowry Acid Strength of Metal Hydride and Dihydrogen Complexes. *Chem. Rev.* **2016**, *116*, 8588–8654.

(58) Waidmann, C. R.; Miller, A. J. M.; Ng, C.-W. A.; Scheuermann, M. L.; Porter, T. R.; Tronic, T. A.; Mayer, J. M. Using Combinations of Oxidants and Bases as PCET Reactants: Thermochemical and Practical Considerations. *Energy Environ. Sci.* **2012**, *5*, 7771.

(59) Kolmar, S. S.; Mayer, J. M. $SmI_2(H_2O)_n$ Reduction of Electron Rich Enamines by Proton-Coupled Electron Transfer. *J. Am. Chem. Soc.* **2017**, *139*, 10687–10692.

(60) Chciuk, T. V.; Flowers, R. A. Proton-Coupled Electron Transfer in the Reduction of Arenes by SmI_2–Water Complexes. *J. Am. Chem. Soc.* **2015**, *137*, 11526–11531.

(61) Chciuk, T. V.; Anderson, W. R.; Flowers, R. A. Proton-Coupled Electron Transfer in the Reduction of Carbonyls by Samarium Diiodide–Water Complexes. *J. Am. Chem. Soc.* **2016**, *138*, 8738–8741.

(62) Chciuk, T. V.; Anderson, W. R.; Flowers, R. A. High-Affinity Proton Donors Promote Proton-Coupled Electron Transfer by Samarium Diiodide. *Angew. Chemie Int. Ed.* **2016**, *55*, 6033–6036.

(63) Chciuk, T. V.; Anderson, W. R.; Flowers, R. A. Interplay between Substrate and Proton Donor Coordination in Reductions of Carbonyls by SmI_2–Water Through Proton-Coupled Electron-Transfer. *J. Am. Chem. Soc.* **2018**, *140*, 15342–15352.

(64) Darcy, J. W.; Kolmar, S. S.; Mayer, J. M. Transition State Asymmetry in C–H Bond Cleavage by Proton-Coupled Electron Transfer. *J. Am. Chem. Soc.* **2019**, *141*, 10777–10787.

(65) Ashida, Y.; Arashiba, K.; Tanaka, H.; Egi, A.; Nakajima, K.; Yoshizawa, K.; Nishibayashi, Y. Molybdenum-Catalyzed Ammonia Formation Using Simple Monodentate and Bidentate Phosphines as Auxiliary Ligands. *Inorg. Chem.* **2019**, *58*, 8927–8932.

(66) Pontes, F. V. M.; Carneiro, M. C.; Vaitsman, D. S.; da Rocha, G. P.; da Silva, L. I. D.; Neto, A. A.; Monteiro, M. I. C. A Simplified Version of the Total Kjeldahl Nitrogen Method Using an Ammonia Extraction Ultrasound-Assisted Purge-and-Trap System and Ion Chromatography for Analyses of Geological Samples. *Anal. Chim. Acta* **2009**, *632*, 284–288.

(67) Saigne, C.; Kirchner, S.; Legrand, M. Ion-Chromatographic Measurements of Ammonium,

Fluoride, Acetate, Formate and Methanesulphonate Ions at Very Low Levels in Antarctic Ice. *Anal. Chim. Acta* **1987**, *203*, 11–21.

(68) Kim, Y.; Deng, H.; Gallucci, J. C.; Wojcicki, A. Rhenium Polyhydride Complexes Containing $PhP(CH_2CH2CH2PCy_2)_2$ (Cyttp): Protonation, Insertion, and Ligand Substitution Reactions of ReH_5(Cyttp) and Structural Characterization of ReH_5(Cyttp) and $[ReH_4(\eta^2\text{-}H_2)$(Cyttp)]$SbF_6$. *Inorg. Chem.* **1996**, *35*, 7166–7173.

(69) Huynh, M. T.; Anson, C. W.; Cavell, A. C.; Stahl, S. S.; Hammes-Schiffer, S. Quinone 1 e^- and 2 e^- /2 H^+ Reduction Potentials: Identification and Analysis of Deviations from Systematic Scaling Relationships. *J. Am. Chem. Soc.* **2016**, *138*, 15903–15910.

(70) Chalkley, M. J.; Del Castillo, T. J.; Matson, B. D.; Peters, J. C. Fe-Mediated Nitrogen Fixation with a Metallocene Mediator: Exploring pK_a Effects and Demonstrating Electrocatalysis. *J. Am. Chem. Soc.* **2018**, *140*, 6122–6129.

(71) Chalkley, M. J.; Oyala, P. H.; Peters, J. C. Cp* Noninnocence Leads to a Remarkably Weak C–H Bond via Metallocene Protonation. *J. Am. Chem. Soc.* **2019**, *141*, 4721–4729.

(72) Askevold, B.; Friedrich, A.; Buchner, M. R.; Lewall, B.; Filippou, A. C.; Herdtweck, E.; Schneider, S. Reactivity of Iridium(I) PNP Amido Complexes toward Protonation and Oxidation. *J. Organomet. Chem.* **2013**, *744*, 35–40.

(73) Bezdek, M. J.; Guo, S.; Chirik, P. J. Coordination-Induced Weakening of Ammonia, Water, and Hydrazine X–H Bonds in a Molybdenum Complex. *Science* **2016**, *354*, 730–733.

(74) Shih, K.-Y.; Schrock, R. R.; Kempe, R. Synthesis of Molybdenum Complexes That Contain Silylated Triamidoamine Ligands. A μ-Dinitrogen Complex, Methyl and Acetylide Complexes, and Coupling of Acetylides. *J. Am. Chem. Soc.* **1994**, *116*, 8804–8805.

(75) Wang, D.; Loose, F.; Chirik, P. J.; Knowles, R. R. N–H Bond Formation in a Manganese(V) Nitride Yields Ammonia by Light-Driven Proton-Coupled Electron Transfer. *J. Am. Chem. Soc.* **2019**, *141*, 4795–4799.

(76) Loose, F.; Wang, D.; Tian, L.; Scholes, G. D.; Knowles, R. R.; Chirik, P. J. Evaluation of Excited State Bond Weakening for Ammonia Synthesis from a Manganese Nitride: Stepwise Proton Coupled Electron Transfer Is Preferred over Hydrogen Atom Transfer. *Chem. Commun.* **2019**, *55*, 5595–5598.

(77) Lindley, B. M.; Appel, A. M.; Krogh-Jespersen, K.; Mayer, J. M.; Miller, A. J. M. Evaluating the Thermodynamics of Electrocatalytic N_2 Reduction in Acetonitrile. *ACS Energy Lett.* **2016**, *1*, 698–704.

(78) Bezdek, M. J.; Pappas, I.; Chirik, P. J. Determining and Understanding N-H Bond Strengths in Synthetic Nitrogen Fixation Cycles; Springer, Cham, 2017; pp 1–21.

(79) Scheibel, M. G.; Abbenseth, J.; Kinauer, M.; Heinemann, F. W.; Würtele, C.; De Bruin, B.; Schneider, S. Homolytic N-H Activation of Ammonia: Hydrogen Transfer of Parent Iridium Ammine, Amide, Imide, and Nitride Species. *Inorg. Chem.* **2015**, *54*, 9290–9302.

TOC Graphic

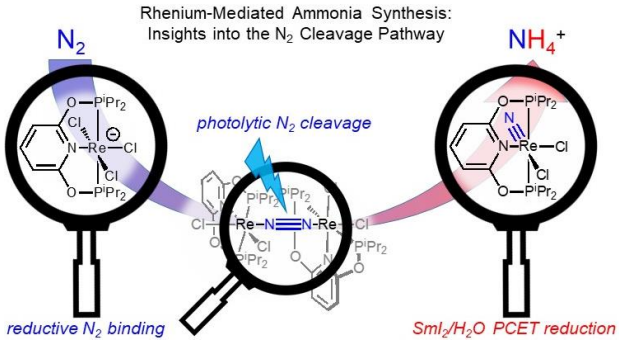
Rhenium-Mediated Ammonia Synthesis:
Insights into the N_2 Cleavage Pathway
N_2
NH_4^+
photolytic N_2 cleavage
reductive N_2 binding
SmI_2/H_2O PCET reduction